
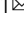





Plasmonic hot electron induced layer dependent anomalous Fröhlich interaction in InSe

Mahfujur Rahaman ¹, Muhammad Awais Aslam ¹, Lu He ¹, Teresa I. Madeira¹ & Dietrich R. T. Zahn ¹

Despite the great promise of InSe for electronic and optoelectronic applications, Fröhlich interaction plays an important role in electrical transport due to the polar nature of it, which can become more significant in reduced dimensionality. Here, we report on how the dimensionality influences the strength and nature of the Fröhlich polaronic effect in InSe with the aid of plasmonic hot electrons injection. Polar optical phonons couple to hot electrons via the Fröhlich interaction in InSe and enable us to monitor them in conventional Raman measurements. We observed that the intensity of these phonon modes initially increases gradually with decreasing layer number and then drops drastically from 7 L to 6 L (transition from quasi-direct to indirect bandgap at room temperature). Additionally, a gradual decrease of intensity of the polar modes with further decreasing layer number is observed due to the increasing indirect bandgap nature of InSe suggesting reduced Fröhlich coupling below this thickness.

¹Semiconductor Physics, Chemnitz University of Technology, Chemnitz, Germany. email: mahfujur.rahaman@physik.tu-chemnitz.de

Among all 2D semiconductors, InSe (a member of metal monochalcogenides) has emerged as an outstanding candidate for post-silicon electronic devices. It possesses a high electron mobility ($\sim 10^3 \text{ cm}^2 \text{ V}^{-1} \text{ s}^{-1}$) due to its small effective mass ($\sim 0.14 m_e$) at room temperature (RT)¹. Even though 2D black phosphorus has a comparable mobility², it is extremely unstable in environmental conditions³, which limits the possibility of practical applications. The large surface-to-volume ratio and the atomic thickness of 2D materials make them ideal for electrostatic control and significant device downscaling for high-density integration⁴. Moreover, the ultraclean, dangling bond free smooth surfaces of these materials are less sensitive to carrier scattering. They can thus outperform existing silicon devices in the regime of scaling limitation. Therefore, InSe provides a promising playground for studying low dimensional phenomena and for developing high mobility nano-electronics^{4,5}.

One of the limiting factors of intrinsic mobility are the phonons, quanta of lattice vibration perturbing the electron potential in a lattice. In polar materials, optical phonons couple strongly with elementary charges due to long-range Coulomb interactions induced by the macroscopic polarization field resulting from the atomic displacement, known as Fröhlich interaction⁶. Therefore, scattering with optical phonons limits the mobility in 2D semiconductors at RT significantly^{7,8}. Intriguingly, 2D Fröhlich interaction is markedly different from its bulk analog as reported in a recent theoretical work⁹. The Fröhlich interaction in 2D materials diverges from the 3D one at zero phonon-momentum limit creating van Hove singularities, where it transforms into a very large finite value compared to the standard electron-phonon coupling (EPC). As a consequence, due to the reduced dielectric screening, the enhanced macroscopic field created by the phonon-assisted polarization density may lead to a stronger EPC in ultrathin materials resulting in a layer-dependent Fröhlich potential and hence device performance. Therefore, the question of how the dimensionality influences the Fröhlich interaction in InSe has great significance and importance for both fundamental understanding and device application. Very recently, Ma et al.⁷ and Li et al.¹⁰ laid the theoretical ground for understanding the 2D model of Fröhlich potential and layer-dependent Fröhlich interaction in InSe by means of intrinsic carrier mobility. To the best of our knowledge, no experimental investigation of layer-dependent Fröhlich interaction in 2D semiconductors, in particular for InSe, has been reported until now.

To accomplish this goal, a systematic investigation of layer-dependent Fröhlich interaction in InSe via the injection of plasmonic hot electrons was performed. Plasmonic nanostructures have outstanding light-trapping and electromagnetic field-confining properties and can generate hot electrons with energies up to 4 eV when excited at localized surface plasmon resonance (LSPR)¹¹. These highly energetic electrons can escape from the plasmonic structures and be collected by the conduction band (CB) of adjacent semiconductors depending on the energy barrier at the interface. The small Schottky barrier (0.1–0.9 eV) of InSe with noble metals is, therefore, an ideal system for the collection of hot electrons from the plasmonic structures^{12,13}. In polar semiconductors, the electric field carried by the free carrier plasmons (here the hot electrons collected by the CB of InSe) interact with the long-range macroscopic field of the longitudinal optical phonons (LO) breaking the Raman selection rules¹⁴. Therefore, Raman spectroscopy can directly measure coupled modes¹⁵ enabling the investigation of the polar LO phonons via plasmonic hot electrons doping as a function of InSe layer number.

InSe studied in this work belongs to the commercially available rhombohedral γ -type crystal structure with an ABC stacking sequence and no centrosymmetry¹⁶. The unit cell consists of three

tetra-atomic layers, in which each tetra-atomic layer (Se-In-In-Se) creates the monolayer of InSe¹⁷. The thickness of each monolayer is 0.8 nm. Bulk InSe is a direct bandgap (E_g) semiconductor¹⁸. However, when thinned down to below 20 layer (20 L) the valence band maxima forms a ‘Mexican hat’ like structure centered at the Γ point with the energy difference between the two maxima and the center minimum smaller than the thermal activation energy at RT¹⁹. Therefore, it remains a quasi-direct bandgap semiconductor down to a certain thickness at RT. Like other layered semiconductors, its bandgap can be tuned upward by as large as ~ 1.0 eV from 1.2 eV in bulk to 2.1 eV in monolayer¹⁸. One notable characteristic of InSe is that it has large optical anisotropy near E_g : the electronic transitions associated with polarization of incident light parallel to the c axis ($E \parallel c$) are two orders of magnitude larger than that perpendicular to c axis ($E \perp c$)^{18,20}. In contrast the electronic transition at around 2.42 eV (E_1 electronic transition) is optically allowed in the normal incident geometry ($E \perp c$). The E_1 gap also exhibits a layer dependence varying from 2.42 to 3.04 eV from bulk to monolayer, respectively¹⁸.

Being a member of the $R3m$ space group with four atoms per monolayer, there are twelve normal modes of vibrations in γ -InSe. Group theory predicts $4A_1$ and $4E$ modes at the Γ point for γ -InSe and apart from the acoustic A_1 and E ones all other modes are Raman and infrared active, but with quite different intensities²¹. Among them, two modes with A_1 and E symmetry are strongly polar and therefore lead to strong infrared absorption. However, at resonant Raman conditions, when the excitation energy matches the E_1 electronic transition, the q -dependent A_1 (LO) mode around 200 cm^{-1} is enhanced dramatically²². When performing Raman measurements far below the E_1 transition in a plasmonic environment, in which the excitation energy approaches the LSPR (surface enhanced Raman scattering (SERS) conditions), we were able to observe three phenomena. These are: (i) appearance of two polar modes A_1 (LO) and E (LO) around 200 and 210 cm^{-1} for InSe, (ii) the intensity of both polar modes are layer dependent with the E (LO) mode having a stronger sensitivity to layer thickness, and (iii) a drastic intensity reduction of the polar modes for the InSe layer number decreasing from 7 to 6 L, which correlates directly to the transition point from quasi-direct to indirect bandgap at RT^{19,23}. Using the combination of different experiments on a large number of samples (>20), we confirm that the appearance of both polar LO modes is due to the Fröhlich coupling with the injected plasmonic hot electrons. The experimental evidence was further confirmed by finite element method (FEM) simulations of the plasmonic coupling between metal nanostructures and InSe using COMSOL.

Our work provides a clear picture of layer-dependent Fröhlich interaction induced EPC in InSe and offers great prospect in the design and optimization of next generation high mobility nano-electronics/optoelectronics. It also opens up the possibility of applications in photovoltaics²⁴ and photocatalysis²⁵.

Results and discussion

Resonant Raman induced Fröhlich interaction in InSe. Figure 1a presents a sample sketch with metal nanotriangles (NTs) on top of InSe flakes. Here, we used Ag, Au, and Al for the coupling between InSe and the plasmon of the metal NTs. Hexagonal arrays of the metal NTs have LSPR in the visible range, which can be tuned via changing the material, size, shape, or dielectric environment^{26,27}.

A typical scanning electron microscope (SEM) image of the sample after nanosphere lithography (NSL) using Ag is shown in Fig. 1b. As can be seen, Ag formed NTs homogeneously covering InSe without damaging the flake. Figure 1c–f are the optical

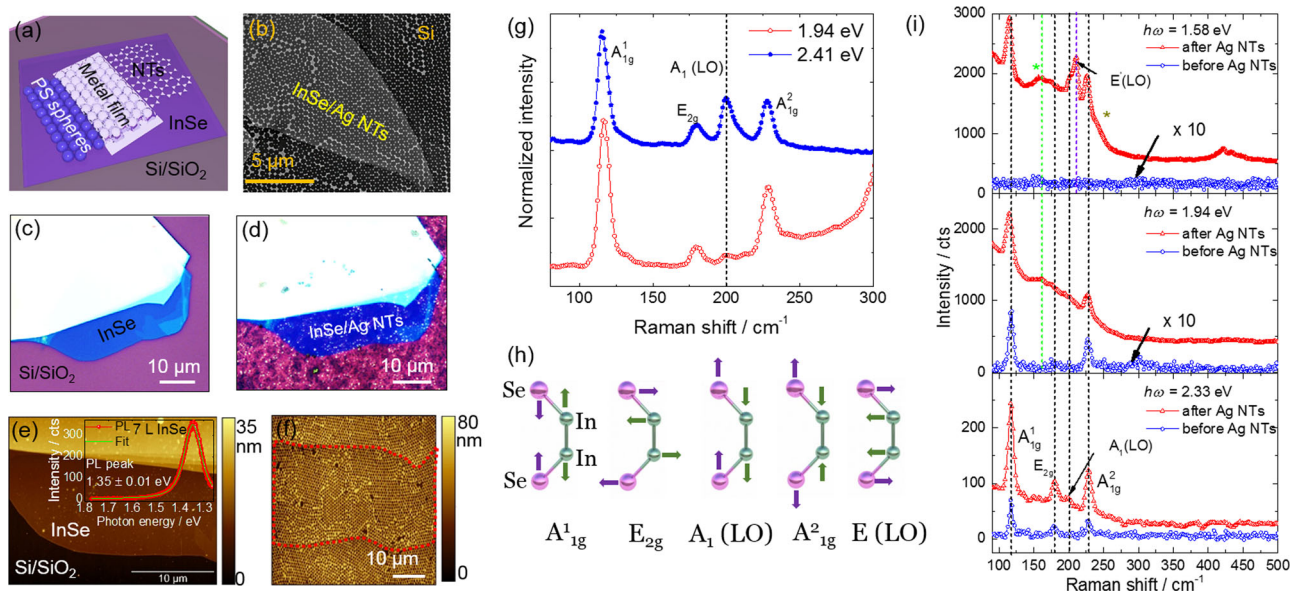


Fig. 1 Optical and morphological characterization of InSe samples. **a** Schematic representation of the sample preparation. Polystyrene spheres of 400 nm size were used for nanosphere lithography (NSL). Ag, Au, and Al were used for nanotriangles (NTs) formation. **b** A typical scanning electron microscope (SEM) image of the InSe sample after Ag NT deposition. Silicon with native oxide was used as substrate for SEM to avoid charging effects. **c, d** Optical images and **e, f** atomic force microscope (AFM) topographies of one typical InSe sample with different thicknesses before and after NSL with Ag, respectively. Inset of **(e)** displays the photoluminescence spectra of 7 layer (7 L) InSe with a Voigt fitting. The red dashed lines in **(f)** marks the area of the thin flake as shown in the optical images. **g** Resonant and nonresonant Raman spectra acquired with 2.41 and 1.94 eV, respectively, of 7 L InSe. Acquisition time for the Raman measurements were 10 s \times 2 and 30 s \times 10, respectively, and the laser power in both measurements were \sim 100 μ W. **h** Elongation patterns of the phonon vibrations visible in the Raman spectra. **i** Raman spectra of 7 L InSe before and after NSL with Ag acquired with 1.58, 1.94, and 2.33 eV excitations. The broad spectral feature between 150 and 190 cm^{-1} is due to the presence of E_{2g} and contribution of In_2O_3 (green dashed line and asterisk). The gray asterisk indicates a feature assigned to amorphous Se. Acquisition time for the measurements were 5 s \times 2 and the laser power was 10 μ W.

images and atomic force microscope (AFM) topographies of one of the InSe samples with different layer thicknesses on a 300 nm SiO_2/Si substrate. Like other layered semiconductors, InSe has a well-known layer-dependent optical bandgap^{18,28}. We thus determined the InSe layer number using the photoluminescence (PL) peak position. The details of thickness determination via PL peak position are presented in the Supplementary note 1. The PL spectrum of 7 L InSe is shown in the inset of Fig. 1e. Using Voigt fitting the PL peak is determined to be centered at (1.35 ± 0.01) eV corresponding to 7 L InSe in good agreement with the literature²⁸. Before turning our attention to the plasmonic hot electron induced Fröhlich interaction, we investigated nonresonant and near-resonant Raman scattering spectra of InSe. This helps in the evaluation of polar modes in InSe since, at resonance excitation, Raman scattering is dominated by the exciton-LO phonon Fröhlich interaction²².

Figure 1g displays both nonresonant and resonant Raman spectra of 7 L InSe measured at 1.94 and 2.41 eV excitation, respectively. In the nonresonant Raman spectrum, we observed three prominent first order Raman modes around 114, 178, and 225 cm^{-1} assigned to A^1_{1g} , E_{2g} , and A^2_{1g} modes, respectively, (see Fig. 1h) according to the irreducible representation of the symmetry group C_{3v}^5 (γ -InSe)²⁹. There is another in-plane E_{2g} mode around 40 cm^{-1} for InSe, which is inaccessible in our experiment. Additionally, we can also observe a very weak contribution of the polar A_1 (LO) around 200 cm^{-1} , while the increasing background around 300 cm^{-1} is the contribution from Si 2nd order phonon scattering. Interestingly, under near-resonant Raman condition when excited by the 2.41 eV laser, the energy of which is close to the E_1 gap (around 2.42 eV) of InSe, together with the nonpolar Raman modes, we observed a dramatic enhancement of the polar modes (asymmetric feature

around 200 cm^{-1}). The peak centered at 200 cm^{-1} can be assigned to A_1 (LO) and the shoulder on the higher frequency side around 210 cm^{-1} to E (LO), both of them are more active in the infrared absorption than in the ordinary Raman spectra^{21,30,31}. However, under near-resonant Raman excitation q -dependent scattering dominates and dictates the Raman symmetry selection rules³². Therefore, infrared active polar phonons are enhanced in the Raman spectra of InSe with strong A_1 (LO) and weaker E (LO) contributions in backscattering geometry.

Plasmonic hot electron induced Fröhlich interaction in InSe.

Figure 1i shows the Raman spectra of 7 L InSe ($E_g = 1.35$ eV) without and with Ag NTs. While the Raman spectra of InSe without Ag NTs show first order Raman modes at 2.33 and 1.94 eV excitations, no Raman modes are observed under 1.58 eV excitation. This could be due to the excitation energy, which is far away from the E_1 and the Raman scattering is less efficient near weakly allowed E_g . In contrast, the Raman spectra of InSe/Ag NTs system exhibit significant modifications. First, we observed the strongest SERS enhancement at 1.58 eV excitation. This is unexpected taking our recent work into account since we showed that hexagonally packed Ag NTs of the same geometry on a SiO_2/Si substrate have a LSPR around 1.9 eV and are thus resonant with 1.94 eV excitation²⁶. However, the present investigation clearly shows that the 1.58 eV excitation is closer to resonance if not at resonance with LSPR of Ag NTs suggesting a shift of the LSPR to lower energies due to the change of dielectric environment in the presence of few layer InSe at the bottom²⁷. Thanks to the resonant SERS effect, together with first order Raman modes we can now observe the polar modes in InSe at 1.58 eV excitation. The broad feature between 150 and 190 cm^{-1} is the combination

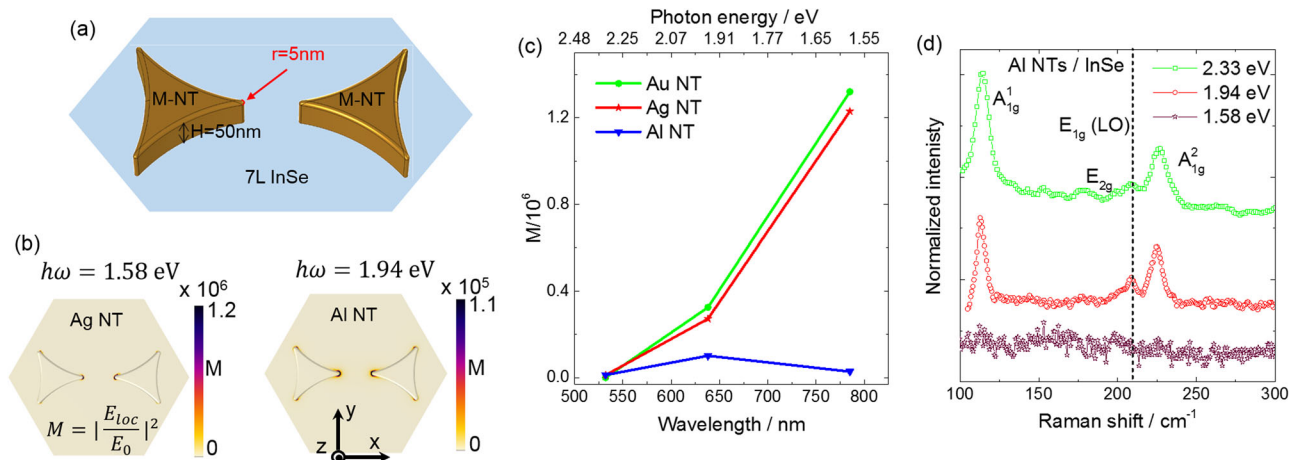


Fig. 2 Finite element method (FEM) simulation of plasmonic coupling between InSe and metal nanotriangles (NTs). **a** Sketch of the model used in the FEM simulation of InSe/metal NTs. **b** Simulated electric field intensity M distribution at two different wavelengths for Ag and Al NTs. Simulated transmittance spectra of InSe/Ag, Au, and Al NTs systems for the spectral range from 380 to 1200 nm together with M distribution for Au NTs at 1.58 eV excitation are presented in Supplementary note 3. **c** Absolute value of calculated maximum M at three different excitations. A similar plasmonic behavior is expected for Ag and Au NTs on InSe for three selected wavelengths while InSe with Al NTs shows a maximum at 1.94 eV excitation. **d** Raman spectra of 7 L InSe with Al NTs acquired under three different wavelengths. As expected from simulations we can resolve the polar modes of InSe best at 1.94 eV excitation. Raman spectra of InSe with Au NTs are presented in Supplementary note 3.

of in-plane E_{2g} mode of InSe and the contribution from In_2O_3 (a byproduct of oxidation in ultrathin InSe)^{33,34}.

To understand the role of InSe on the LSPR of metal NTs, we performed FEM simulations using COMSOL multiphysics 5.6 in 3D platform. Figure 2a presents the model used to simulate the experimental geometry studied in this work. Details of the 3D model can be found in the methods section and Supplementary note 2. The transmittance spectra of the three metal NTs (Au, Ag, Al) on 7 L of InSe computed in the spectral range from 360 nm (3.44 eV) to 1200 nm (1.03 eV) are presented in Supplementary note 2 (Fig. S2a). The distribution of the electric field intensity enhancement M around the Ag and Al NTs calculated at 1.58 and 1.94 eV excitations, respectively, are shown in Fig. 2b. The M distribution for Au NTs at 1.58 eV excitation can be found in Supplementary note 2 (Fig. S2b). As expected, the corners of the NTs generate the strongest electric field enhancement in agreement to previous works^{26,35}. The absolute values of the calculated maximum M for Ag, Au, and Al NTs at three different wavelengths are displayed in Fig. 2c. From Fig. 2c and Supplementary note 2 (Fig. S2a), we can see that Au and Ag NTs show strongest enhancement under 1.58 eV excitation compared to the other two energies. Therefore, excitation with 1.58 eV shall produce a stronger plasmonic field and generate highly energetic hot electrons in both metal NTs. This result thus confirms that the strongest enhancement in the Raman spectra of InSe with Ag or Au NTs should appear at 1.58 eV excitation (Raman spectrum of InSe/Au NTs at 1.58 eV excitation is presented in Supplementary note 2 (Fig. S2c)). Under this excitation condition the two polar modes (A_1 (LO) and E (LO)) are observed in the Raman spectra.

From the simulation results shown in Fig. 2c and Supplementary note 2 it is clear that the LSPR of Al NTs shifts towards 638 nm (1.94 eV) and one should expect the strongest plasmonic enhancement effect at 1.94 eV excitation. Figure 2d presents Raman spectra of InSe with Al NTs acquired at all three excitation wavelengths. Indeed we observe the strongest plasmonic enhancement at 1.94 eV excitation in terms of the appearance of the two polar modes. No Raman features are visible at 1.58 eV since this excitation energy is nonresonant for both the InSe and the LSPR of Al NTs. Please note that the Raman spectra of InSe at

2.33 eV excitation is the combination of plasmonic enhancement and near-resonant Raman effect as discussed above.

One notable difference between the near-resonant Raman spectra in Fig. 1g and the SERS spectra at 1.58 eV excitation in Fig. 1i is the relative intensity ratio between A_1 (LO) and E (LO). In the case of near-resonant Raman excitation, the A_1 (LO) mode appears much stronger compared to the E (LO) one in agreement with literature^{21,36,37}. On the contrary, the E (LO) mode is more enhanced than the A_1 (LO) mode in resonant SERS spectra, in which the probability of generated hot electron in NTs collected by InSe is the maximum, consistently in the present study. This is likely due to hot carrier induced EPC of the E (LO) polar mode being much stronger in InSe as suggested in a recent DFT investigation³⁸. Additionally, our simulation shows that the stronger in-plane plasmonic field component at 1.58 eV excitation (see Supplementary note 2 (Fig. S2d)) couples to the in-plane E (LO) mode better than A_1 (LO) mode resulting in enhanced relative intensity.

The Raman spectra presented in Figs. 1i and 2d clearly indicate that the plasmonic coupling between InSe and metal NTs is the sole contributor to the observation of the polar modes in the Raman spectrum excited by 1.58 and 1.94 eV, which would be nonresonant without NTs. There are two possible plasmonic phenomena, which can contribute to the observation of the polar modes: (i) the local field strongly confined at the corners of NTs as shown in Fig. 2b and Supplementary note 2 (Fig. S2d) and (ii) injection of the plasmonic hot electrons. A similar behavior was also observed for the case of a monolayer MoS_2 /Au nanodisc system in our previous work³⁹. The strongly confined plasmonic field in a monolayer MoS_2 sandwiched by a nanodisc and a sharp metallic tip generated hot electrons, which excite an infrared active A_{2u} mode under 1.58 eV excitation energy, far below the bandgap of the monolayer MoS_2 .

To test our hypothesis, we partially encapsulated InSe by a few layers of hBN (~10 L) and deposited Ag NTs using the same procedure. The plasmonic field decays exponentially through the hBN capping layer with a decay constant (see Supplementary note 3) and hBN blocks InSe from being doped by plasmonic hot electrons. Therefore, we are able to determine the influence of the two effects mentioned above on hBN capped InSe directly.

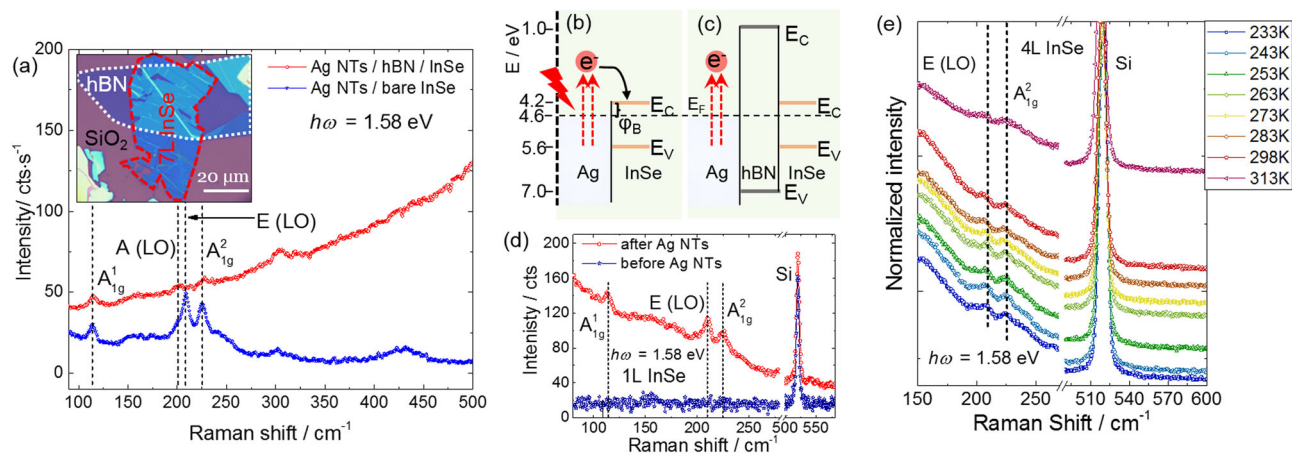


Fig. 3 Effect of charge carriers and bandgap on Fröhlich interaction in InSe. **a** Raman spectra taken with 1.58 eV excitation of hBN encapsulated and bare InSe/Ag NTs demonstrating the influence of plasmonic hot electron doping. The inset is the optical image of the partially encapsulated sample used for the measurements. The areas marked by the white dotted and red dashed lines indicate hBN and InSe, respectively. **b, c** Simplified diagram of the band alignment illustrating the hot electron injection process. **b** InSe with Ag nanotriangles (NTs), **c** InSe/hBN/Ag NTs. The values are taken from the refs. 13, 40, 41. **d** Raman spectra of monolayer (1L) InSe before and after Ag NTs deposition. The bandgap of 1L InSe is well above the excitation energy at 1.58 eV. **e** Temperature-dependent Raman measurements of 4L InSe/Ag NTs at 1.58 eV excitation. The acquisition parameters of the Raman measurements are $30 \text{ s} \times 2$ (7L) and $150 \text{ s} \times 2$ (1L), $10 \mu\text{W}$ under $\times 100$, 0.9 NA objective. The acquisition parameters for the temperature-dependent Raman measurements were $150 \text{ s} \times 2$, $10 \mu\text{W}$ under $\times 50$, 0.45 NA objective.

Figure 3a displays an optical image of the heterostructure showing bare and hBN encapsulated InSe regions together with two representative Raman spectra of the two regions after Ag NTs deposition using 1.58 eV excitation. The Raman spectra of bare InSe in the presence of Ag NTs exhibits a strong contribution of the polar modes as well as enhancement of the nonpolar modes in agreement with the results shown in Fig. 1i. However, the intensities of the nonpolar first order Raman modes display weaker enhancement for hBN encapsulated InSe with Ag NTs than without Ag NTs, since we did not observe any Raman features in the absence of Ag NTs at 1.58 eV excitation as demonstrated in Fig. 1i. The weak enhancement of the nonpolar Raman modes can be due to the screening of the plasmonic field by the hBN interlayer. The effect of this weak plasmonic coupling can also be observed through the enhanced PL (by a factor of 5.4) from hBN encapsulated InSe after Ag NTs deposition (see Supplementary note 3), which also leads to an increased background in the red spectrum in Fig. 3a.

For bare InSe with Ag NTs, on the other hand, we did not observe any PL. This is likely due to the efficient exciton dissociation known to occur at the semiconductor/metal interface³⁷. However, the hBN capping blocks the exciton dissociation from InSe to the Ag NTs. Therefore, we can observe the PL enhancement via plasmonic coupling. The Raman spectra taken from the hBN encapsulated InSe with Ag NTs show negligible contribution from the polar modes, especially the E(LO) mode. This is a stark contrast to the nonpolar Raman modes in hBN capped InSe. The appearance of a much weaker A₁(LO) mode in hBN capped InSe indicates that the contribution of local plasmonic field gradient induced selection rules (as discussed above) may aid to the weak appearance of A₁(LO) mode. On the other hand, the vanishing E(LO) mode suggests that the plasmonic hot electron doping plays the critical role in activating the polar modes in nonresonant Raman spectra for InSe.

Figure 3b, c depict approximated band alignment diagrams for the heterostructures shown in Fig. 3a indicating the injection of the plasmonic hot electrons mechanism in InSe. The values needed to construct the band alignment were taken from the literature^{13,40,41}. After excitation at LSPR, the plasmon can decay radiatively or non-radiatively by transferring the energy to the

conduction electrons in the metal nanostructures. This process creates highly energetic hot electrons, which can escape from the metal and be collected by a semiconductor in contact with the plasmonic structures. The energy transferred to the hot electrons from the noble metal nanostructures at LSPR excitation is higher than 1 eV and can reach up to 4 eV¹¹. Therefore, hot electrons generated in Ag NTs can easily overcome the barrier height ϕ_B (~ 0.4 eV) and dope InSe. When encapsulated by hBN, this wide bandgap insulator creates a blocking layer for the hot electrons to be collected by InSe (Fig. 3c). As a result, polar modes in InSe are weak in the red spectrum of Fig. 3a.

One of the critical sources of the Fröhlich interaction in polar semiconductors is the intraband EPC stemming from the scattering of charges within the same valence or conduction band (CB) by LO phonons. Injection of plasmonic hot electrons in InSe meets such criteria since electrons escaping the metal nanostructures are collected by the CB of InSe. These in turn interact with the long-range macroscopic polarization density associated with either the creation or annihilation of LO phonons in InSe⁷. The charge transport driven by an electric field through InSe can also be influenced by such a macroscopic field, which consequently reduces the mobility.

Even though the electronic transition at the bandgap in InSe is weak at normal incidence, it can still induce resonant Raman scattering in a strong plasmonic field. Hence, the strong intensity of the polar phonons observed in 7L InSe may also be activated via this resonance phenomenon. To examine this scenario, we prepared a 1L InSe with Ag NTs sample. The PL spectra of the flake confirming the layer thickness is presented in Supplementary note 4. The bandgap of 1L InSe at RT is 2.1 eV, i.e. 1.58 eV excitation is well below the electronic transition. Therefore, if the appearance of the polar phonons would only stem from the coupling between these phonons and the weakly allowed E_g transition in a strong plasmonic field, we should not observe them for 1L InSe. Instead, the polar phonons in 1L InSe when covered with Ag NTs are clearly observed (Fig. 3d).

Furthermore, by conducting a temperature-dependent Raman investigation on two selected thicknesses (4L: $E_g \geq 1.58$ eV and 7L: $E_g < 1.58$ eV at RT) of InSe with Ag NTs at 1.58 eV excitation, it becomes clear that with decreasing temperature the bandgap of

4 L (7 L) InSe moves away (towards) from the excitation energy of 1.58 eV, i.e. the resonance condition is tuned correspondingly. The result for 4 L InSe is presented in Fig. 3e and for 7 L InSe in Supplementary note 5. As depicted in Fig. 3e, the Raman signatures of polar E (LO) and nonpolar A_{1g}^2 phonons in 4 L InSe are visible in the spectra and their intensities remain constant throughout the temperature range (233–313) K. Due to strong increasing Rayleigh background the A_{1g}^1 mode around 114 cm^{-1} could not be observed under $\times 50$, 0.45 NA objective used for the temperature-dependent study. The constant intensity of the E (LO) mode over the whole temperature range indicates that the activation of polar phonons in InSe at 1.58 eV excitation does not depend on the E_g transition.

On the other hand, the temperature-dependent Raman spectra of 7 L InSe/Ag NTs at 1.58 eV excitation presented in Supplementary note 5 reveal that the intensity of polar phonons is enhanced when the temperature-dependent bandgap approaches the excitation energy at lower temperature. This is because with decreasing temperature the bandgap of 7 L InSe approaches the excitation energy of 1.58 eV meaning resonance with E_g is established. This phenomenon suggests that the fundamental bandgap E_g plays a role in enhancing the polar LO modes. However, as we showed in this work hot electron injection is the prerequisite for observing the polar LO modes, thus Fröhlich interaction in InSe takes place.

Layer dependent evolution of Fröhlich interaction in InSe.

Figure 4 depicts the layer dependent Raman spectra of InSe with Ag NTs with corresponding PL spectra acquired prior to NTs deposition. As can be seen, the intensity of the polar modes (especially the E (LO) mode) gradually increases from bulk to 7 L of InSe, where it reaches a maximum. This is likely due to the resonant condition since, with decreasing layer number the bandgap of InSe approaches the excitation energy of 1.58 eV. After that, there is a drastic drop of intensity of the E (LO) mode at 6 L InSe, which then continues to decrease gradually with further decreasing layer number. The corresponding PL spectra in Fig. 4b clearly reveal that the transition from direct to indirect bandgap at RT also occurs from 7 to 6 L InSe. Details of the layer

dependent bandgap evolution in InSe are discussed in Supplementary note 1.

In a polar semiconductor, free carrier plasmons couple to LO phonons via the interaction between the macroscopic electric field associated with LO phonons and the electric field induced by the free carriers. The strength of this coupling together with several other factors depends on the nature of the bandgap since conduction-electron plasmons couple strongly to the LO phonon in a direct bandgap semiconductor due to the formation of an electron gas with small effective mass and large dielectric constant¹⁵. According to recent DFT investigations of layer dependent optoelectronic properties of InSe, the electron effective mass in the CB minima also increases with decreasing layer number due to strong interlayer coupling associated with the P_z hybridized orbitals of both In and Se atoms^{10,42}. Therefore, one can expect a reduced electron-LO phonon coupling in thinner flakes of InSe. Even though this hypothesis could explain the gradual decrease of the Fröhlich interaction below 6 L InSe, the sudden drop of intensity of the polar modes from 7 to 6 L (the transition point of direct to indirect bandgap) suggests that the nature of the bandgap plays a crucial role as well. To understand the role of electron effective mass, change of dielectric environment, and nature of bandgap on layer-dependent Fröhlich coupling in InSe, more detailed theoretical studies are needed, which are beyond the scope of this work.

Note that the bandgap is increasing with decreasing layer number in InSe, which also increases the barrier height at the InSe/Ag interface. This may also influence the hot electron injection probability. However, considering the fact that the hot electrons can gain large energy in Ag nanostructures¹¹, a barrier height of $<1\text{ eV}$ to InSe can easily be overcome. Additionally, the LSPR of Ag NTs shall move to higher energy with decreasing thickness of InSe, especially for very thin flakes, resulting in different coupling between InSe and Ag NTs.

To understand how the LSPR compares at different thicknesses we calculated the local electric field enhancement due to Ag NTs for 2 nm InSe (representing 2 L InSe) at 1.58 eV excitation energy. The simulation results are presented in Supplementary note 6. The local electric field enhancement of Ag NTs on 2 L InSe and 7 L InSe are comparable, i.e. the sharp intensity decrease of polar

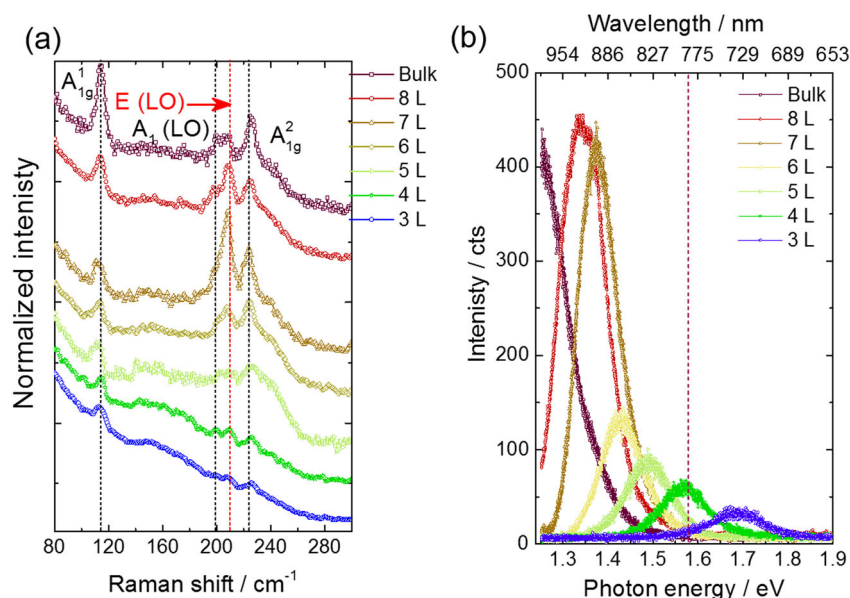


Fig. 4 Layer-dependent Fröhlich interaction in InSe. Layer dependent (a) Raman spectra excited at 1.58 eV and (b) corresponding photoluminescence spectra of InSe. There is a drastic drop of intensity of the polar LO modes from 7 to 6 L corresponding to the thickness where the direct to indirect bandgap transition of InSe occurs.

phonons at ultrathin flakes cannot be explained by a change of the LSPR of Ag NTs. Therefore, the decreasing intensity of the polar phonons below 6 L InSe is due to the reduced Fröhlich coupling as is clearly indicated in Fig. 4a.

This is a very important result and critical since the Fröhlich interaction strongly suppresses the mobility of the charge carriers thus reducing any device performance. The reported sequence of procedure, experimental results, simulations and cross referenced interpretations provide a clear picture of the layer-dependent Fröhlich interaction mechanism occurring in InSe, which is relevant in future device applications of this promising 2D material. We also performed laser power dependent Raman measurement on bare InSe on SiO₂ substrate under 1.58 eV excitation to investigate if it is possible to observe the polar modes with increasing laser power. The Raman results are presented in Supplementary note 7. As can be seen with increasing laser power we are able to monitor the first order Raman modes in InSe. However, no polar modes were visible. This could be due to the strong optical anisotropy at the band edge of E_g at normal incidence in InSe resulting in less efficient electron pumping to the CB.

Conclusion

We studied the Fröhlich interaction in InSe by monitoring the strength of polar LO modes induced by injected plasmonic hot electrons. We deposited three metal (Al, Ag, and Au) nanostructures on InSe and excited the heterostructure system near LSPR. The laser lines (1.58 and 1.94 eV) used in this work are far away from the electronic transition energy at E_1 , i.e. far away from the resonant-Raman condition for InSe. We observed the strong appearance of polar LO modes of InSe in resonant SERS condition, which are otherwise very weak in ordinary Raman conditions. The combination of the strong local field at the corners of the NTs and the hot electrons generated due to near LSPR excitation activates and enhances these polar phonon modes enabling their observation in the Raman measurements. We performed FEM simulations to calculate the plasmonic coupling between InSe and metal NTs. We observed an excellent agreement between the simulation and experiments showing that the polar LO modes are only observed when the excitation energy approaches the LSPR (the condition for the largest concentration of hot electrons excited in the metal nanostructures). To elucidate our findings further, we conducted a series of experiments including a repetition of the SERS experiments on hBN encapsulated InSe, which confirmed that the plasmonic hot electron doping is the origin of the polar modes appearing in the spectra. Finally, we investigated the layer-dependent Fröhlich interaction in InSe. We found that intensity of polar modes initially increases with decreasing layer number indicating increasing Fröhlich coupling. The sudden decrease of intensity of the polar modes from 7 to 6 L coincides with the transition from direct to indirect bandgap at RT. The polar mode intensities gradually decrease with further decreasing layer number. The reduction of the intensity of the polar modes suggests that the Fröhlich coupling is smaller for thinner flakes below 7 L due to the indirect bandgap nature. Our results provide an experimental picture of layer-dependent Fröhlich coupling in InSe, which is vital for any potential device application of this promising material.

Methods

Sample preparation. The InSe material used in this work is undoped and was purchased from 2D Semiconductors, USA. Thickness dependent InSe samples were prepared using a PDMS assisted deterministic dry transfer method onto SiO₂ (300 nm)/silicon substrates⁴³. After transferring the flakes, self-assembled monolayers of polystyrene spheres of 400 nm size were used for NSL creating a hexagonally packed metal (Ag, Au, Al) arrays of NTs with ~120 nm side length and ~50 nm height on the sample surface. Details of the deposition technique can be found

elsewhere²⁶. Prior to the dry transfer, PL spectra were acquired for each flake for thickness determination.

PL and Raman measurements. A Horiba Xplora plus system equipped with an electron multiplying charge couple detector (EMCCD) was used for both PL and Raman measurements at normal incidence. PL measurements were carried out using a 532 nm (2.33 eV) excitation. Raman spectra of InSe were acquired in backscattering geometry using 532 nm (2.33 eV), 638 nm (1.94 eV), and 785 nm (1.58 eV) excitations and a 1200 l/mm grating was used to disperse the Raman signals onto the EMCCD. A $\times 100$, 0.9 NA objective was used to excite and collect the signals for both PL and Raman measurements. The laser powers of 100 and ~10 μ W were employed at the sample surface for PL and Raman measurements, respectively. The spectral acquisition times were different for different measurement sets and stated in the respective result sections.

Resonant Raman spectra of multilayer InSe at E_1 transition (2.42 eV) were acquired under 514.7 nm (2.41 eV) excitation using a Horiba LabRam HR800, a symphony CCD detector, and 600 l/mm grating. A $\times 100$, 0.9 NA objective was used to excite and collect the signal and the laser power was 100 μ W at the sample surface.

Temperature-dependent Raman measurement were carried out using a liquid nitrogen cooled Linkam stage and 1.58 eV laser excitation in the Xplora plus system with the aid of a $\times 50$, 0.45 NA objective.

Finite element method simulation. FEM simulations of InSe/metal NTs were performed using COMSOL multiphysics 5.6 in 3D platform in the wavelength domain. The dimension of the NTs were set according to the experimental conditions (side length: 120 nm, height: 50 nm). In order to avoid a singularity problem and to have an optimal approach to real conditions, edges and corner of the NTs were rounded with a radius of curvature of 5 nm. The 7 L InSe on 300 nm SiO₂ is modeled as a 7 nm thick InSe layer. The optical constants of InSe⁴⁴, Ag⁴⁵, Au⁴⁵, and Al⁴⁶ were taken from the literature.

SEM and AFM measurements. SEM images were taken using a SEM (FEI Nova NanoSEM 200) with an accelerating voltage of 10 kV, and 5 mm working distance in immersion mode (high-resolution mode). AFM topography images were acquired using a AIST-NT scanning probe microscope in intermittent contact mode. Commercially available Si cantilevers were used for the AFM measurements.

Data availability

All data generated and analyzed during this investigation are available from the corresponding author upon reasonable request.

Received: 1 March 2021; Accepted: 8 July 2021;

Published online: 30 July 2021

References

1. Bandurin, D. A. et al. High electron mobility, quantum Hall effect and anomalous optical response in atomically thin InSe. *Nat. Nanotechnol.* **12**, 223–227 (2017).
2. Li, L. et al. Black phosphorus field-effect transistors. *Nat. Nanotechnol.* **9**, 372–377 (2014).
3. Island, J. O., Steele, G. A., Zant, H. S. Jvd & Castellanos-Gomez, A. Environmental instability of few-layer black phosphorus. *2D Mater.* **2**, 011002 (2015).
4. Feng, W., Zheng, W., Gao, F. & Hu, P. Atomically thin InSe: a high mobility two-dimensional material. *Sci. China Technol. Sci.* **60**, 1121–1122 (2017).
5. Feng, W., Zheng, W., Cao, W. & Hu, P. Back gated multilayer InSe transistors with enhanced carrier mobilities via the suppression of carrier scattering from a dielectric interface. *Adv. Mater.* **26**, 6587–6593 (2014).
6. Fröhlich, H. Electrons in lattice fields. *Adv. Phys.* **3**, 325–361 (1954).
7. Ma, J., Xu, D., Hu, R. & Luo, X. Examining two-dimensional Fröhlich model and enhancing the electron mobility of monolayer InSe by dielectric engineering. *J. Appl. Phys.* **128**, 035107 (2020).
8. Lugovskoi, A. V., Katsnelson, M. I. & Rudenko, A. N. Strong electron-phonon coupling and its influence on the transport and optical properties of hole-doped single-layer InSe. *Phys. Rev. Lett.* **123**, 176401 (2019).
9. Sohler, T., Calandra, M. & Mauri, F. Two-dimensional Fröhlich interaction in transition-metal dichalcogenide monolayers: theoretical modeling and first-principles calculations. *Phys. Rev. B* **94**, 085415 (2016).
10. Li, W., Poncé, S. & Giustino, F. Dimensional crossover in the carrier mobility of two-dimensional semiconductors: the case of InSe. *Nano Lett.* **19**, 1774–1781 (2019).
11. Clavero, C. Plasmon-induced hot-electron generation at nanoparticle/metal-oxide interfaces for photovoltaic and photocatalytic devices. *Nat. Photonics* **8**, 95–103 (2014).

12. Hu, S. et al. Au–InSe van der Waals Schottky junctions with ultralow reverse current and high photosensitivity. *Nanoscale* **12**, 4094–4100 (2020).
13. Sun, H., Wang, Z. & Wang, Y. Band alignment of two-dimensional metal monochalcogenides MXs (M=Ga,In; X=S,Se,Te). *AIP Adv.* **7**, 095120 (2017).
14. Varga, B. B. Coupling of plasmons to polar phonons in degenerate semiconductors. *Phys. Rev.* **137**, A1896–A1902 (1965).
15. Yuasa, T. et al. Raman scattering from coupled plasmon-LO-phonon modes in n-type AlxGal-xAs. *Phys. Rev. B* **33**, 1222–1232 (1986).
16. Leisgang, N. et al. Optical second harmonic generation in encapsulated single-layer InSe. *AIP Adv.* **8**, 105120 (2018).
17. Hao, Q. et al. Phase identification and strong second harmonic generation in pure ε-InSe and its alloys. *Nano Lett.* **19**, 2634–2640 (2019).
18. Brotons-Gisbert, M. et al. Nanotexturing to enhance photoluminescent response of atomically thin indium selenide with highly tunable band gap. *Nano Lett.* **16**, 3221–3229 (2016).
19. Mudd, G. W. et al. The direct-to-indirect band gap crossover in two-dimensional van der Waals Indium Selenide crystals. *Sci. Rep.* **6**, 39619 (2016).
20. Mazumder, D. et al. Enhanced optical emission from 2D InSe Bent onto Si-Pillars. *Adv. Optical Mater.* **8**, 2000828 (2020).
21. Sánchez-Royo, J. F. et al. Electronic structure, optical properties, and lattice dynamics in atomically thin indium selenide flakes. *Nano Res.* **7**, 1556–1568 (2014).
22. Ashokan, S., Jain, K. P., Balkanski, M. & Julien, C. Resonant Raman scattering in quasi-two-dimensional InSe near the M0 and M1 critical points. *Phys. Rev. B* **44**, 11133–11142 (1991).
23. Hamer, M. J. et al. Indirect to direct gap crossover in two-dimensional InSe revealed by angle-resolved photoemission spectroscopy. *ACS Nano* **13**, 2136–2142 (2019).
24. Atwater, H. A. & Polman, A. Plasmonics for improved photovoltaic devices. *Nat. Mater.* **9**, 205–213 (2010).
25. Mukherjee, S. et al. Hot electrons do the impossible: plasmon-induced dissociation of H₂ on Au. *Nano Lett.* **13**, 240–247 (2013).
26. Rahaman, M., Moras, S., He, L., Madeira, T. I. & Zahn, D. R. T. Fine-tuning of localized surface plasmon resonance of metal nanostructures from near-Infrared to blue prepared by nanosphere lithography. *J. Appl. Phys.* **128**, 233104 (2020).
27. Duval Malinsky, M., Kelly, K. L., Schatz, G. C. & Van Duyne, R. P. Nanosphere lithography: effect of substrate on the localized surface plasmon resonance spectrum of silver nanoparticles. *J. Phys. Chem. B* **105**, 2343–2350 (2001).
28. Song, C. et al. Largely tunable band structures of few-layer InSe by uniaxial strain. *ACS Appl. Mater. Interfaces* **10**, 3994–4000 (2018).
29. Tamalampudi, S. R. et al. Thickness-dependent resonant Raman and E' photoluminescence spectra of indium selenide and indium selenide/graphene heterostructures. *J. Phys. Chem. C* **123**, 15345–15353 (2019).
30. Gasanly, N. M., Yavador, B. M., Tagirov, V. I. & Vinogradov, E. A. Infrared and Raman spectra of layer InSe single crystals. *Phys. Status Solidi* **89**, K43–K48 (1978).
31. Kuroda, N. & Nishina, Y. Resonant Raman scattering at higher M0 exciton edge in layer compound InSe. *Solid State Commun.* **28**, 439–443 (1978).
32. Martin, R. M. Theory of the one-phonon resonance raman effect. *Phys. Rev. B* **4**, 3676–3685 (1971).
33. Liu, D. et al. Large-scale synthesis of hexagonal corundum-type In₂O₃ by ball milling with enhanced lithium storage capabilities. *J. Mater. Chem. A* **1**, 5274–5278 (2013).
34. Shi, L. et al. Oxidation mechanism and protection strategy of ultrathin indium selenide: insight from theory. *J. Phys. Chem. Lett.* **8**, 4368–4373 (2017).
35. Murray, W. A., Suckling, J. R. & Barnes, W. L. Overlayers on silver nanotriangles: field confinement and spectral position of localized surface plasmon resonances. *Nano Lett.* **6**, 1772–1777 (2006).
36. Molas, M. R. et al. Raman spectroscopy of GaSe and InSe post-transition metal chalcogenides layers. *Faraday Discussions*, <https://doi.org/10.1039/D0FD00007H> (2021).
37. Lei, S. et al. Evolution of the electronic band structure and efficient photo-detection in atomic layers of InSe. *ACS Nano* **8**, 1263–1272 (2014).
38. Chen, Z. et al. Ultrafast dynamics of hot carriers in a quasi-two-dimensional electron gas on InSe. *Proc. Natl Acad. Sci.* **117**, 21962 (2020).
39. Milekhin, A. G. et al. Giant gap-plasmon tip-enhanced Raman scattering of MoS₂ monolayers on Au nanocluster arrays. *Nanoscale* **10**, 2755–2763 (2018).
40. Schulman, D. S., Arnold, A. J. & Das, S. Contact engineering for 2D materials and devices. *Chem. Soc. Rev.* **47**, 3037–3058 (2018).
41. Wickramaratne, D., Weston, L. & Van de Walle, C. G. Monolayer to bulk properties of hexagonal boron nitride. *J. Phys. Chem. C* **122**, 25524–25529 (2018).
42. Sun, Y. et al. InSe: a two-dimensional material with strong interlayer coupling. *Nanoscale* **10**, 7991–7998 (2018).
43. Castellanos-Gomez, A. et al. Deterministic transfer of two-dimensional materials by all-dry viscoelastic stamping. *2D Mater.* **1**, 011002 (2014).
44. Adachi, S. *The Handbook on Optical Constants of Semiconductors*. (WORLD SCIENTIFIC, 2012).
45. Johnson, P. B. & Christy, R. W. Optical constants of the noble metals. *Phys. Rev. B* **6**, 4370–4379 (1972).
46. McPeak, K. M. et al. Plasmonic films can easily be better: rules and recipes. *ACS Photonics* **2**, 326–333 (2015).

Acknowledgements

We acknowledge funding by the German Science Foundation DFG via DFG ZA 146/44-1, and the SMWK/ESF (RL ESF Hochschule und Forschung 2014-433 2020 mit Antragsnummer 100380093) projects for supporting the research work. We also thank Ms. Doreen Dentel of Solid Surfaces Analysis group in Chemnitz for the SEM measurements.

Author contributions

M.R. and M.A.A. performed the measurements and analysis the date. M.R. and D.R.T.Z. involved in the evaluation and interpretation of the results. M.R., L.H., and T.M. developed the simulation model and performed the calculations. M.R. wrote the manuscript. All authors contributed to the understanding of the experimental findings and writing the manuscript.

Funding

Open Access funding enabled and organized by Projekt DEAL.

Competing interests

The authors declare no competing interests.

Additional information


Supplementary information The online version contains supplementary material available at <https://doi.org/10.1038/s42005-021-00674-5>.

Correspondence and requests for materials should be addressed to M.R.

Peer review information *Communications Physics* thanks the anonymous reviewers for their contribution to the peer review of this work. Peer reviewer reports are available.

Reprints and permission information is available at <http://www.nature.com/reprints>

Publisher's note Springer Nature remains neutral with regard to jurisdictional claims in published maps and institutional affiliations.

 **Open Access** This article is licensed under a Creative Commons Attribution 4.0 International License, which permits use, sharing, adaptation, distribution and reproduction in any medium or format, as long as you give appropriate credit to the original author(s) and the source, provide a link to the Creative Commons license, and indicate if changes were made. The images or other third party material in this article are included in the article's Creative Commons license, unless indicated otherwise in a credit line to the material. If material is not included in the article's Creative Commons license and your intended use is not permitted by statutory regulation or exceeds the permitted use, you will need to obtain permission directly from the copyright holder. To view a copy of this license, visit <http://creativecommons.org/licenses/by/4.0/>.

© The Author(s) 2021